VICTORIA UNIVERSITY
MELBOURNE AUSTRALIA

Structural effects on SAPO-34 and ZIF-8 materials exposed to seawater solutions, and their potential as desalination membranes

This is the Accepted version of the following publication

Structural effects on SAPO-34 and ZIF-8 materials exposed to seawater solutions, and their potential as desalination membranes

Mikel Duke[1], Bo Zhu[1], Cara M. Doherty[2], Matthew Hill[2], Anita J. Hill[2,3] and Moises A. Carreon[4]

[1]Institute for Sustainability and Innovation, College of Engineering and Science, Victoria University, Werribee Campus, PO Box 14428, Melbourne, VIC, Australia, 8001, bo.zhu@vu.edu.au, mikel.duke@vu.edu.au

[2]Manufacturing, The Commonwealth Scientific and Industrial Research Organization (CSIRO), Private Bag 10, Clayton South, VIC, Australia, 3169, cara.doherty@csiro.au matthew.hill@csiro.au, anita.hill@csiro.au

[4] Chemical and Biological Engineering Department, Colorado School of Mines, Golden CO, 80401,USA.

mcarreon@mines.edu

Abstract

The effects of saline water on the material properties of two promising salt rejecting structures, SAPO-34 and ZIF-8, were explored for desalination. Immersing SAPO-34 in seawater revealed a release of Al which involved some replacement by Ca, K, Mg and Na. X-ray powder diffraction revealed a robust structure in deionised and sea water solutions. ZIF-8 on the other hand, lost 1% of its mass due to release of Zn into both deionised water and seawater solutions, yet structure remained intact. N_2 and positron annihilation lifetime spectroscopy porosimetry techniques revealed loss of surface area and mesopores on both materials, explained by capillary forces acting to close them. Membrane reverse osmosis revealed no liquid water flux for SAPO-34 due to the intactness of the membrane and very small pore size which contributed to prohibitive resistance to liquid water flow. ZIF-8 membranes permeated water, but did not demonstrate significant salt rejection indicating that either the slight mass loss impacted membrane integrity to reject salt, or that liquid water diffusion in ZIF-8 does not follow a salt rejecting path. SAPO-34 and ZIF-8 structures are stable structures for aqueous applications including sea salts, but further work is needed to develop them for reverse osmosis desalination.

1. Introduction

Increased urbanisation and climate change are putting pressures on our fresh water resources [1]. In finding solutions to ensure secure supply of fresh water for communities and industry, a range of options have been considered, which include water recycling and seawater desalination. While conventional reverse osmosis membranes made from polyamide are low cost and readily available, they are not stable under more challenging environments such as heat (>50°C), oxidants such as chlorine and extremes of pH. Inorganic and organic/inorganic hybrid materials can offer these

1

properties, but the material must possess the essential functional feature to pass water molecules and block ions (i.e. desalination). Materials which possess these properties and have already been demonstrated for desalination are silica [2, 3] and zeolites [4-9]. Seawater desalination was demonstrated in reverse osmosis mode on MFI type zeolite membranes, which have an intrinsic crystal pore size of 0.55nm [10]. In saline waste water desalination, MFI type zeolite membranes were shown to produce high quality water suitable for reuse, and exhibited strong tolerance to cleaning with high strength chlorine [11]. Zeolite HS has also been considered for reverse osmosis desalination, having cavity diameters of 0.66nm separated by apertures of 0.3nm and 0.22nm [12]. Alternatively, microporous crystalline materials such as zeolite SAPO-34 (a silicoaluminophosphate with chabazite (CHA) type framework), and zeolitic imidazolate framework (ZIF-8) have been successfully prepared as membranes for diverse molecular gas separations, but to the best of our knowledge are yet not tested for reverse osmosis in water treatment.

The model for permeating water molecules (0.276 nm) through SAPO-34 and ZIF-8 structures is shown in Figure 1. Here we see their sizes with respect to the size of the two model hydrated ions, Na^+ (0.716 nm) and Cl^- (0.664 nm) [13], which are abundant in many saline water sources (e.g. seawater, groundwater and waste water). SAPO-34 is a silicoaluminophosphate having the composition $(Si_xAl_yP_z)O_2$ where x = 0.01–0.98, y = 0.01–0.60, z = 0.01–0.52, and $x + z = y$ [14] and unimodal micropore size of 0.38 nm is a potential appealing candidate for desalination. Zeolitic imidazolate frameworks (ZIFs) [15-18] a subclass of metal organic frameworks (MOFs), have emerged as a novel type of crystalline porous materials which combine highly desirable properties, such as uniform micropores, high surface areas, and exceptional thermal and chemical stability, making them ideal candidates for diverse functional applications. Even more recently different ZIF compositions have been prepared as defect free membranes by independent research groups [19-27]. These membranes have demonstrated the ability to separate molecular mixtures of gases. In particular, ZIF-8 (Composition $Zn(MeIM)_2$), is known to be highly stable in aqueous environments [15, 28] and thus a suitable candidate for water treatment application. To validate ZIF-8 as a candidate for a desalination membrane material, Hu and co-workers simulated that it possesses the correct intrinsic porosity to permeate water, but block Na^+ and Cl^- ions [29]. The concept for this mechanism is highlighted by the size of the ZIF-8 aperture relative to the water and ions is shown in Figure 1.
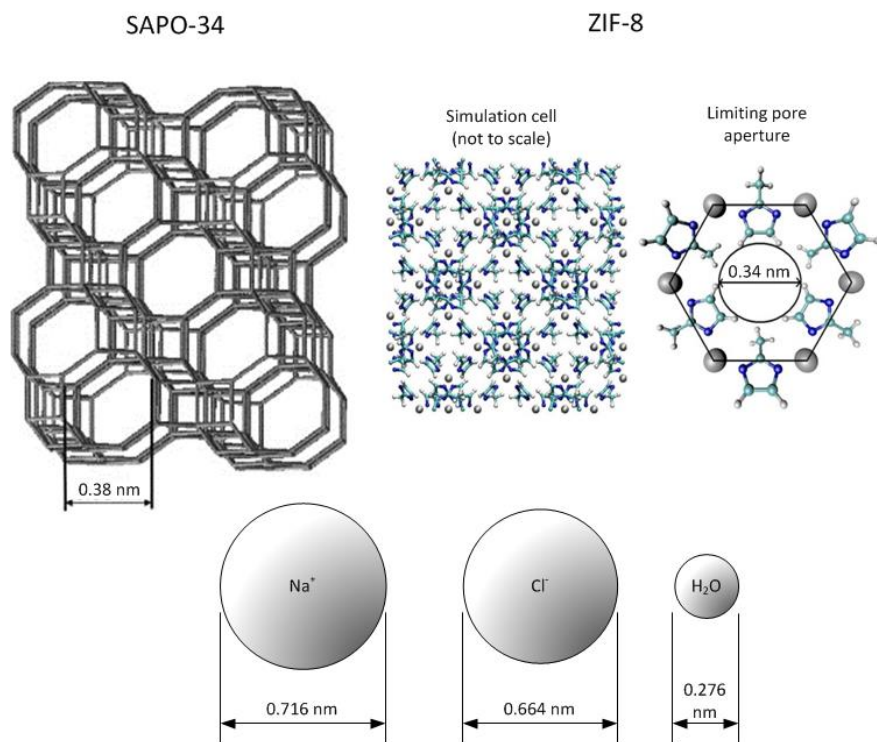
Figure 1: Relative sizes of SAPO-34 (chabazite) and ZIF-8 structures as compared to the hydrated ions Na$^+$ and Cl$^-$ and a water molecule. SAPO-34 and ZIF-8 structures modified from Li et al [30] and Hertäg et al. [31] respectively, and ion hydrated diameters from Nightingale [13].

Despite this promising progress in the field of membrane science, and also the promise of SAPO-34 and ZIF-8 to function in water treatment and desalination, it is important to first understand how these materials behave in the presence of ions. In previous work, we explored the uptake of ions within MFI-type zeolite structures known to be effective as desalination membranes [32]. We found a dynamic feature of ion exchange that involved the ultimate expulsion of monovalent cations (Na$^+$ and K$^+$), replaced by divalent cations (Ca^{2+} and Mg^{2+}). Structurally, this meant the MFI underwent expansion or contraction upon the exchange detected by powder XRD and Rietveld refinement. With this, we were able to conclude that K$^+$ and the infusion of divalent cations had a marked effect on the zeolite crystalline pores as well as grain boundaries which ultimately explained the dynamic behaviour of zeolite desalination membranes where salt rejections slowly reach high numbers (>90%) due to the blockage of pores with large, more strongly bound, divalent cations.

In this work, we aim to explore the novel application of SAPO-34 and ZIF-8 (both as crystals and membranes) materials for desalination. We explore the structural effects of SAPO-34 and ZIF-8 upon exposure to the model seawater mixtures (representing a realistic ion balance in ocean environments). Results from ion adsorption, X-ray powder diffraction and positron annihilation lifetime spectroscopy (PALS) will be used to align ion uptake/release events with structural differences after water exposure. We then present desalination performance results on SAPO-34 and ZIF-8 membranes that we can correlate with the structural information.

3

2. Experimental

Synthesis of SAPO-34 and ZIF-8 crystals

SAPO-34 crystals

To make SAPO-34 crystals, 5.1 g of aluminum isopropoxide (Al(i-C$_3$H$_7$O)$_3$, >99.99% metal basis, Aldrich), 2.9 g of phosphoric acid (H$_3$PO$_4$, 85 wt %, Aldrich), and 13.12 g of deionized H$_2$O were stirred for 2 h to form a homogeneous solution. Then, 0.56 g of Ludox AS-40 colloidal silica (SiO$_2$, 40 wt %, Sigma-Aldrich) was added, and the resulting solution was stirred for 3 h. To this solution, 5.27 g of tetraethylammonium hydroxide ((C$_2$H$_5$)$_4$NOH, 35 wt %, Sigma-Aldrich) were added, and the resultant solution was stirred for another 0.5 h. Finally, 2.05 g of dipropylamine (C$_6$H$_{15}$N, 99%, Aldrich) were added, and the solution was aged for 3 days at 50°C under vigorous stirring. The gel molar composition was: 1Al$_2$O$_3$:1.33P$_2$O$_5$:0.16SiO$_2$:1TEAOH:1.6DPA:77H$_2$O. The solution was placed in a sealed Teflon-lined autoclave (Parr Instrument Company) under autogenous pressure and treated hydrothermally at 220°C for 24 h in a conventional oven. After the solution was cooled to room temperature, it was centrifuged at 4000 rpm for 20 min to separate the seeds and the seeds were then washed with deionized water. Centrifugation-washing process was repeated three times. The resultant precipitate was dried overnight at 70°C. The template was removed by calcination using flowing air in a computer-controlled muffle furnace, using a ramp procedure at heating and cooling rates of 1 °C /min and 10 °C /min respectively.

ZIF-8 crystals

To make ZIF-8 crystals, 0.3 g of zinc nitrate hexahydrate, (Zn(NO$_3$)$_2$ 6H$_2$O, Fluka, ≥99%) was dissolved in 11.3 g of methanol (Acros Organics, extra dry, water <50 ppm). A solution consisting of 0.66 g of 2-methylimidazole (C$_4$H$_6$N$_2$, Aldrich, 99%) and 11 g of methanol was added to the Zn based solution and vigorously stirred for 24 h. The solids were separated by centrifugation at 4000 rpm for 20 min and washed with methanol. This procedure was repeated three times. The resultant ZIF-8 powder was dried overnight at 100°C.

Pure water and seawater exposure on SAPO-34 and ZIF-8 powders

SAPO-34 and ZIF-8 powders were subjected to pure deionised water (DI Water) and synthetic seawater solution made from sea salts (Aldrich) and DI Water made to 38,000 mg/L to replicate the concentration of the ocean. The supplied salts contain a range of ions including trace elements, but the system was set up to detect Al, Ca, K, Mg, Na and Zn. 2.5mL of DI Water or seawater was added together with 0.5g of SAPO-34 or ZIF-8 powder sample. Cation analysis was performed by inductively coupled plasma-optical emission spectrometry (ICP-OES) (Shimadzu ICPE-9000). All powder samples where characterised by N$_2$ adsorption, X-ray powder diffraction and the more novel positron annihilation lifetime spectroscopy as described below.

N$_2$ adsorption

The N$_2$ adsorption experiments were carried out using a Tri Star 3000 porosity analyser (Micromeritics, USA) at liquid N$_2$ temperature on the original and exposed (DI water or seawater) powder samples degassed for 4 h at 150 °C.

X-ray powder diffraction (XRD)

Powder XRD patterns were collected using a Bruker D8-Discover diffractometer at 40 kV, 40 mA with Cu Kα radiation.

Positron annihilation lifetime spectroscopy (PALS)

PALS measurements were undertaken using EG&G Ortec fast-fast coincidence spectrometers and a 30 μCi ^{22}NaCl positron source, sealed in 2.54 μm Mylar. Prior to analysis, the powder samples were degassed overnight at 150˚C. 2 mm of powder was packed each side of the sealed positron source and placed under vacuum for measurement (5×10^{-7} Torr). A minimum of five files of 4.5×10^6 integrated counts were collected for each sample. The data was analysed using LT (version 9) software and was best fitted with five lifetime components and one source correction component (1.607 ns and 2.634%). Lifetime 1 (τ_1) was fixed to 125 ps due to para positronium annihilation events and τ_2 was attributed to free positron annihilation (~400 ps). Therefore 3 components (τ_{3-5}) were associated with ortho-positronium annihilation within the intrinsic, micro and meso pores of the samples. The average pore diameter for τ_3 and τ_4 was determined using the Tao-Eldrup model [33, 34] while the pore size for τ_5 was calculated using the rectangular Tao-Eldrup (RTE) model [35].

Scanning electron microscopy

The morphology of SAPO-34 and ZIF-8 crystals was inspected using a scanning electron microscopy (SEM) Nova NanoSEM 600 FEI with an acceleration voltage of 10 kV.

Membrane fabrication

SAPO-34 membranes

SAPO-34 membranes were prepared according to our previous report [36]. Briefly, two SAPO-34 membranes were synthesized by secondary seeded growth inside tubular porous stainless steel supports (0.1 grade, 0.27-*μ*m pores, Mott Corporation). The tubes were 6 cm long and had an internal/external diameter of 0.6/1.1 cm. The synthesis gel preparation and molar ratios were the same we employed for SAPO-34 crystals synthesis. The membranes were prepared by rubbing the inside surface of porous supports with dry, calcined SAPO-34 crystals using cotton swabs. The rubbed porous supports, with their outside wrapped with Teflon tape, were then placed vertically in an autoclave and filled with synthesis gel. The hydrothermal treatment was carried out at 220°C for 24 h. The resulting membranes were washed with deionized water and dried overnight at 70°C. The membranes were calcined using a computer-controlled muffle furnace at 400°C for 8 h in atmospheric air to remove the organic template. The calcination heating and cooling rates were 0.7 °C /min and 0.9 °C /min respectively. To confirm membrane intactness, gas permeation was conducted using an equimolar mixture of CO_2 and CH_4. The CO_2/CH_4 permselectivity of the SAPO-34 membrane was 159, which is much higher than the ideal Knudsen model value of 0.60, confirming intactness of the CO_2 selective molecular sieving structure. CO_2 permeance was 4.6×10^{-7} mol/m^2/s/Pa.

ZIF-8 membranes

Two ZIF-8 membranes were prepared inside tubular α-alumina supports (0.2 μm pores, US Filter) by secondary seeded growth as reported earlier [19]. The support tubes were 6 cm long and had an internal/external diameter of 0.7/1.1 cm. Before synthesis, about 1 cm on each end of the supports was glazed (Duncan 1001N) to prevent membrane bypass and to provide a sealing surface for *O*-rings. The permeate area was ~5.1 cm^2. The glazed supports were calcined at 900°C for 30 min with controlled heating and cooling rates of 1°C/min and boiled at 100°C for 1 h and dried overnight at 100°C. Membranes were prepared by rubbing the inside surface of the support with dry ZIF-8 crystals and outside wrapped with Teflon tape. The supports were then placed in a Teflon lined stainless steel autoclave and filled with the synthesis gel and treated hydrothermally at 150°C for 5 h. After hydrothermal treatment, the membrane was washed with deionized water and dried for 2 h at 100°C. A second layer was applied similarly by placing the support in opposite direction for uniformity. Then, the double layered membrane was washed with deionized water, dried and stored at 100°C before separation experiments. Intactness of the ZIF-8 membrane was confirmed using gas permeation. CO_2/CH_4 permselectivity was between 1.2 and 1.6 for both membranes which shows CO_2 adsorption selective diffusion within an intact microporous ZIF-8 membrane film. The CO_2 permeances were in the order of 10^{-8} mol/m^2/s/Pa

Membrane desalination testing

Desalination performance of the prepared membranes was carried out in the desalination test system similar to that used in our previous work [10]. The desalination experiments were conducted in a cross-flow setup with the feed solution (deionised water or 3,000 mg/L NaCl) being fed under pressure on the inside and permeating to the outside of the membrane. The operating pressure (up to 700 kPa) was supplied by feeding N_2 into the feed vessel and was maintained constantly during the test. Total flux, J_T, (kg/m^2/h) was calculated according to:

$$J_T = \frac{w}{At}$$

(1)

Where *w* (kg) is the weight of the collected permeate over a given time period, *t* (h), and A the membrane's area (m^2). The quality of the separation was determined by rejection of NaCl, r_{NaCl} (%), across the feed and permeate according to:

$$r_{NaCl} = \frac{(c_{f,NaCl} - c_{p,NaCl})}{c_{f,NaCl}} 100$$

(2)

Where $c_{f,NaCl}$ and $c_{p,NaCl}$ are the feed and permeate concentrations of NaCl in the feed and permeate respectively (in mg/L). These concentrations were determined with a portable conductivity meter (Sension 156, HACH) and by converting the electrical conductivity measurements to concentration values via a pre-determined relationship.

3. Results and discussion

Behaviour of ions in solution in the presence of SAPO-34

Table 1 shows the results for the behaviour of the dissolved ions, Al, Ca, K, Mg, Na and Zn, in the aqueous solution after 48 hours exposure to both DI water and the synthetic seawater. When SAPO-34 comes into contact with DI water, we see the emergence of Al, Ca and K in small amounts (<20 mg/L). The remaining ions were undetected. These ions may be expected as residuals from the synthesis procedure as they are all present in the original chemicals used. Most importantly, this step validated that only small quantities of these loosely bound ions would be released relative to the activity when SAPO-34 comes into contact with seawater.

Table 1: Response to ion concentration in DI water and seawater solutions before and after exposure to SAPO-34 for 48h. 0.5g of powder sample added to 2.5 mL of solution.

Sample	Ionic species concentration (mg/L)					
	Al	Ca	K	Mg	Na	Zn
DI water	<1	<1	<1	<1	<1	<1
DI water + SAPO	17	16	10	<1	<1	<1
Seawater	7.5	415	389	1,330	10,230	<1
Seawater + SAPO-34	770	377	205	1,290	9,870	<1

The changes in ion concentrations when exposed to seawater were quite significant. Al was significantly released into solution, corresponding to 3.8 mg-Al/g sample, where it is not significantly present in seawater. All other ions detected were taken up into SAPO-34, ranging from 3.3% decline in Mg up to 47% decline in K. Na had a low proportionate uptake (3.6%), however exhibited the largest absolute uptake of 364 mg/L (or 1.8 mg-Na/g sample) taken from the original 10,230 mg/L in solution. Likewise, the other monovalent cation, K, was also taken up in relatively large quantity, 184 mg/L from the original 389 mg/L (or 0.92 mg-K/g sample). Thus from this data, we can conclude that SAPO-34 preferably expels the larger Al ions to accommodate smaller divalent, and to a larger extent monovalent ions, into the structure. This is in contrast to MFI-type zeolite where we found that divalent ions were taken in at the expense of monovalent ions at low alumina content [32, 37]. However, it is important to mention that at higher alumina content MFI-type zeolite (ZSM-5) we see similar behaviour, in particular the release of Na [37] suggesting uptake of ions is stronger in higher alumina materials like SAPO-34.

Behaviour of ions in solution exposed to ZIF-8

The change in ion concentrations in the solution with ZIF-8 samples is shown in Table 2. In much the same fashion for SAPO-34, we see that most ions came out of the material into the DI water in low quantities (<20 mg/L) except Zn, for which a substantial amount (>2,000 mg/L) was released. This is an unusual finding and we speculate that this is a result of the release of loosely bound Zn from synthesis into the water sample. The seawater exposure tests confirm the release of the Zn from the ZIF-8 as it is not initially present in the seawater.

Table 2: Response to ion concentration in the DI water and seawater solutions before and after exposure to ZIF-8 after 48h. 0.5g of powder sample added to 2.5 mL of solution.

Sample	Ionic species concentration (mg/L)					
	Al	Ca	K	Mg	Na	Zn
DI water	<1	<1	<1	<1	<1	<1
DI water + ZIF-8	7.4	19	15	<1	<1	2,010
Seawater	7.5	415	389	1,330	10,230	<1
Seawater + ZIF-8	7.6	356	339	1,235	9,000	1,880

In the presence of seawater, we see that ZIF-8 had little involvement with Al. The largest relative change was to Ca (14% reduction). But in absolute terms, Na was more outstanding in terms of uptake, with a Na reduction of more than 1,200 mg/L (or 6.2 mg-Na/g sample). Mg was reduced by 100 mg/L, while Ca and K were reduced by 60 mg/L and 50 mg/L respectively. Besides these uptakes, the only ion to be released was Zn, and in comparable amount to when treated with DI water. So we conclude that the uptake of ions into ZIF-8 appeared to be more alike adsorption as opposed to ion exchange like SAPO-34. This may be possible if the material was charged, but more likely the porous features of ZIF-8 allow for the entry of the anions as well. In this case, the most abundant ions, Mg and Na, were preferred. A value of +55 mV has been reported for the zeta potential of ZIF-8 nanocrystals dispersed in methanol [38] implying that the material exhibits a positive charge and would preferentially attract anions. If this was the case, it would seem that the association with cations and ZIF-8 is weaker. If we look at the charge balance by summing up the charges associated with the change in ion concentration, we see that for SAPO-34, 34% of the charge lost from the release of Al was replaced by the uptake of the remaining ions. Meanwhile ZIF-8 exhibited no exchange phenomena, at least based on the dominant cations examined in this study. In both materials, a substance was released (Al for SAPO-34 and Zn for ZIF-8) which may be of concern if they were to be used in water treatment or environmental applications. We also observed a release of K when exposing MFI-type zeolites to seawater [32]. While these substances may have been released only upon their first contact with aqueous solutions, it does still show that the loss of these substances either by ion exchange or by release from the material structure should be considered over the longer term in their given application.

XRD of SAPO-34 and ZIF-8 exposed to DI water and seawater

The diffraction patterns of both SAPO-34 and ZIF-8 before and after exposure for 48h in DI water and seawater are shown in Figure 2. SAPO-34 did not show any significant changes to the relative heights and intensities of the peaks indicating that only slight changes in crystallinity occurred both under DI water and seawater.
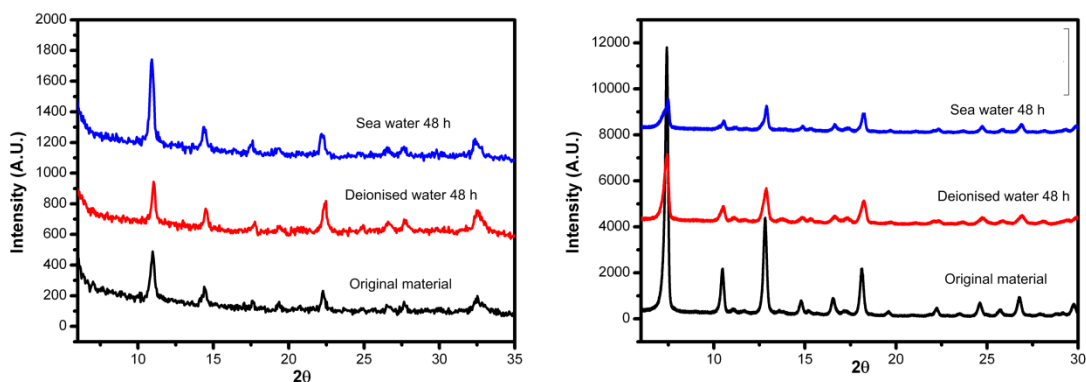
Figure 2: Powder XRD patterns on SAPO-34 (left) and ZIF-8 (right) for samples exposed to DI water or seawater for 48 hours.

ZIF-8 also exhibited little change to the overall structure as the characteristics peaks were present after exposure to both water and seawater. As shown in Table 2 there was a loss of Zn that corresponded to 9.4 mg-Zn/g sample, or just 1% of the total mass of the original ZIF-8 material suggesting a stable material. Pan et al. demonstrated that ZIF-8 is stable even in the presence of boiling water [28], so our result supports the observed stability of the crystal structure of ZIF-8 when exposed to water. Studies of ZIF-8 for aqueous phase drug adsorption and detection proved effective and no change to XRD intensity was observed before and after aqueous solution exposure [39, 40]. However the Zn release measured in our work may be suggestive of some loss of material that could impact the material's function for rejection of hydrated ions when applied as a desalination membrane in reverse osmosis. So it is indeed possible that while adsorption studies in aqueous systems yield positive results, there may be an initial release of Zn from synthesis and corresponding initial loss in some ZIF-8 material, but the remaining material is highly stable.

Considering the chemical formula of ZIF-8 is $C_8H_{10}N_4Zn$, approximately 28.8% corresponds to Zn. This is in agreement with the CHN analysis we have done in the past for ZIF-8: carbon, hydrogen and nitrogen contents in the ZIF-8 framework, C – 41.7%, H - 4.5% and N - 24.4% (ash ~ 29.4%). Ash in this case corresponds to Zn. So 1% total weight loss of Zn is not significant in proportion to the total Zn present in ZIF-8. The mechanism of ZIF-8 degradation in the presence of water cannot be concluded from the current data, but appears insignificant if sorbents are truly stable. However the slight measured loss in structure may be important for defect free membrane films as will be discussed later.

Nitrogen porosimetry

The SAPO-34 and ZIF-8 powders were tested by N_2 adsorption to measure the N_2 accessible (>0.36nm) porous characteristics as shown in Figure 3. The materials all exhibited type-I isotherms, which is typical for microporous materials (pore size < 2nm). ZIF-8 and SAPO-34 showed a slight decrease in N_2 uptake after exposure to DI water and seawater. However the change was associated mostly with the exposure to water, regardless whether it contained ions. Specifically for SAPO-34, slight desorption hysteresis was observed at higher relative pressures, especially $p/p_0 > 0.8$. This is

due to capillaries present in the structure and thus the presence of mesopores. As the reduced N_2 uptake occurred from the very first data point ($p/p^0 = 0.01$), but continued to higher relative pressures following the similar trend, the material maintained the majority of it pores in the micropore and small mesopore domain, and little change occurred to the material at larger pore sizes.
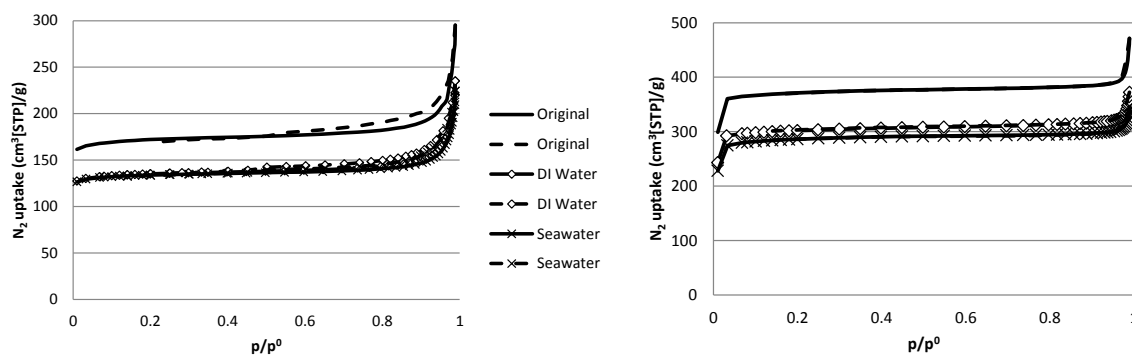

Figure 3: N_2 adsorption and desorption isotherms for SAPO-34 (left) and ZIF-8 (right) sample treated by DI water and seawater. Solid lines represent adsorption branch, while dashed lines represent desorption branch.

The surface area of the samples determined by BET reduction of the isotherms to surface area is shown in Table 3. We see typical surface areas measured for SAPO-34 and ZIF-8 as measured elsewhere. Typical BET specific surface areas for SAPO-34 are in the ~500-700 m^2/g range depending on the calcination temperature and crystal size [41]. For ZIF-8, typical specific surface areas are in the 1000- 1600 m^2/g range, depending on the concentration of residual species (unreacted linker) on the cavities of the framework [15, 19, 38]. The reduction in surface area of SAPO-34 material was around 22% regardless of DI water or seawater exposure. This change could be due to loss of structure, but XRD results in Figure 1 indicate that the SAPO-34 structure was stable. Also, it may not be related to ion exchange because even DI water exposure lead to the area reduction, where ions were not significantly released. So the likely explanation is that the water had an effect to reduce the presence of larger mesopores, possibly by the water's surface tension which assisted in closing the pores and reducing the surface area.

Table 3: BET surface area of SAPO-34 and ZIF-8 samples exposed to DI water and seawater as measured by N_2 adsorption at 77K.

Exposure condition	BET surface area (m^2/g)	
	SAPO-34	ZIF-8
Original	517	1,113
DI water 48 h	406	907
Seawater 48h	401	806

The relative reduction in surface area for ZIF-8 was lower after DI water treatment, dropping by 18%. However seawater reduced the surface area by 28%. Reduction in larger mesopores observed for

SAPO-34 is also likely to occur for ZIF-8, while the material also maintained its crystalline structure (Figure 2).

PALS porosimetry

The multimodal porous structure is conveniently revealed by PALS as shown in Figure 4 for SAPO-34 and in Figure 5 for ZIF-8. The intensity of each lifetime (I_3, I_4 and I_5) is related to the relative number of pores within the sample and the pore diameters are calculated from the lifetimes (τ_3, τ_4 and τ_5). Looking first at SAPO-34, the three lifetimes were 0.741 +/- 0.003 ns, 7.296 +/- 0.193 ns and 42.312 +/- 2.069 ns, corresponding to pore diameters of 0.23 nm, 1.1 nm and 3.4 nm respectively. The relatively large intensity of the third lifetime component, I_3, indicates that the bulk of the porosity of SAPO-34 is made of up the smallest micropores of 0.23 nm (τ_3). Smaller contributions came from larger micropores of 1.1 nm (τ_4) and mesopores of 3.4 nm (τ_5). Determining the hierarchical structure of micropoous inorganic solids by PALS is consistent with previous studies. During work on amorphous microporous silica, five lifetime components were found to provide the best fit of the PALS spectra [42]. The last three are due to ortho-positronium annihilation inside pores, allowing their lifetimes to be translated to a pore size using a quantum based model [35]. The functional pore size responsible for molecular sieving of gases measured by PALS was found to correlate with the cut-off point of permeating gases through membranes made of the same material. The application of PALS has also been successfully utilised for characterising hybrid silica [43]. In the application of zeolites, PALS characterisation found that MFI-type zeolite powder samples had three pore sizes, representing the intrinsic zeolite crystalline micropores, intercrystalline micropores and interparticle mesopores [32, 37]. The technique has since been applied to characterise intact membrane films using PALS and Doppler broadening energy spectroscopy (DBES), which revealed instead only two pore sizes of the zeolite, being the intrinsic and intercrystalline pores of an intact high quality zeolite membrane [44]. Therefore PALS is an effective technique in understanding the intrinsic zeolite pores and the intercrystalline grain boundaries, for both powder samples and membranes.

The 0.23 nm pore size determined by PALS in our work can be associated with the intrinsic pores of the SAPO-34 crystal, but is lower than the expected pore size reported for SAPO-34 of around 0.38 nm [30]. The theoretical size of the zeolite cages are generally determined from the aluminosilicalite structure and do not consider the presence of cations [45]. Therefore the smaller micropores detected using PALS are likely due to the presence of surface species within the pores and are more indicative of the actual pore size. Despite the strong release of Al shown in Table 1, the size of the small pores do not appear to be large enough to accommodate Al (hydrated diameter = 0.950nm [13]). So it is likely that Al occupied the grain boundaries as has been observed for larger divalent cations in MFI [32, 37]. However unlike MFI which has larger intrinsic pores of 0.55nm, for SAPO-34 it appears that the uptake of even Na would also only occur in the grain boundaries as it is only just large enough to accommodate this small cation [46]. A more likely reason for the smaller measured pore size may be the contribution of smaller pores to the calculated average. An exploration of zeolite pore structures by PALS looked at fitting both four and five lifetime components [47]. It was concluded that positrons were also trapped in voids, cages and channel intersections different to the channels, where together with the difference in their geometries to the cylindrical fitting model, explained differences between expected zeolite channel sizes and the pore sizes determined by PALS.
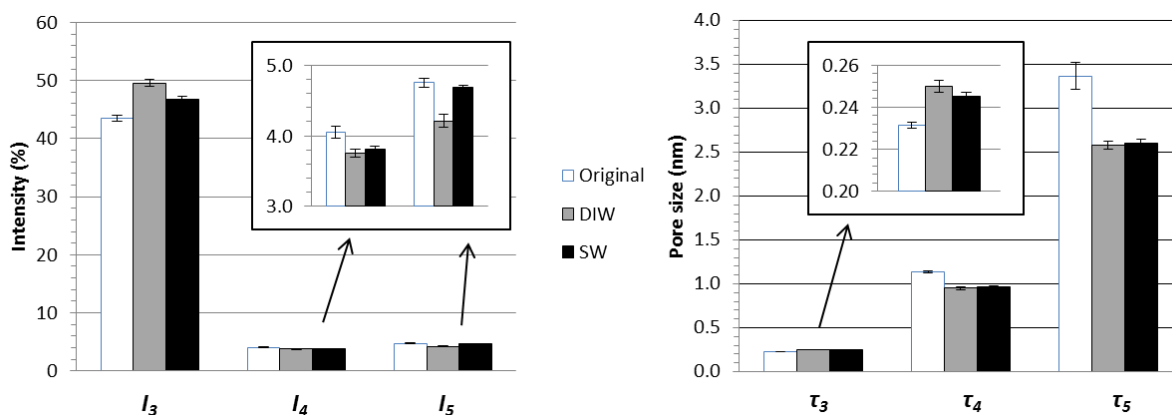
Figure 4: PALS results for the intensities (I_3, I_4 and I_5) and pore sizes calculated from corresponding lifetimes (τ_3, τ_4 and τ_5) of SAPO-34.

Corresponding to the reduction in BET surface area in Tables 2 and 3, we see that PALS detected a reduction in size of the SAPO-34 mesopores (τ_5) and to a lesser extent, the larger micropores (τ_4), upon contact with either DI water or seawater (Figure 4). Meanwhile their respective intensities where slightly reduced. As large pore closure due to capillary forces was concluded earlier, the PALS result indicates that this was due to closure of larger grain boundaries and interparticle mesopores suggesting they were potentially more dynamic than smaller pores which would experience stronger capillary forces. The crystalline pores remained mostly intact (τ_3) also supported by XRD results (Figure 2). In previous work, we observed previously a stronger change (-15%) in the intrinsic pores of low alumina MFI structures, but a negligible change at higher alumina MFI-type zeolite [37]. Therefore SAPO-34 appears to behave like a more structurally robust high alumina MFI-type zeolite.

PALS results showed that the ZIF-8 samples also featured three pore sizes (Figure 5). The three pore sizes were determined from the corresponding three lifetimes of 2.041 +/- 0.494 ns, 6.731 +/- 1.994 ns and 44.427 +/- 1.606 ns respectively. The smallest micropores (τ_3) averaged 0.57 nm, while larger micropores (τ_4) averaged 1.10nm and mesopores (τ_5) averaging 3.53 nm. The small micropore size was considerably larger than the reported aperture size of 0.34 nm [15]. Therefore like SAPO-34, PALS reports contributions of other pores with different sizes. ZIF-8 has been defined as having a pore with the largest sphere fitting into the framework of 1.16nm [48]. A van der Waals radius of 1.2Å for the hydrogens dominating the surface was used to estimate the pore size. The larger micropore size correlated with the size of the largest sphere that can fit into the framework, but for the smaller micropores it is likely that the positrons accumulate inside all the interconnected pores and are showing an average pore size larger than the aperture size shown in Figure 1. Also, occupancy of ions within some larger micropores is likely to reduce their pore size. However this is difficult to determine due to the large and inconclusive loss of Zn. If free Zn was indeed present from ZIF-8 synthesis, it would occupy all pore spaces, including the intrinsic pores, which is another reason why 0.57nm was measured for an intrinsic pore potentially as large as 1.16nm. So for the larger pore ZIF-8 with the loss of Zn upon exposure to water, increasing volume of intrinsic pores and larger micropores (I_3 and I_4 respectively) together with the decreasing average size (τ_3 and τ_4 respectively) implies a rise in pore volume of smaller pores that were previously occupied by Zn. However the change may also occurred within the accuracy of the I_3 and I_4 values suggesting the possibility of little or no change in these pore domains and hence even more evidence of a structurally intact ZIF-8 crystal. The

mesopores of 3.5 nm (τ_5) can also be occupied by Zn. But loss in volume and size of the mesopores appears similar to SAPO-34 indicating the capillary forces acting to close larger mesopores was more dominant. In any case, the observation that the majority of the pore volumes and sizes were maintained indicate a stable ZIF-8 structure regardless of the observed Zn release, which is further evidence to support the conclusion in an overall stability of the bulk material.
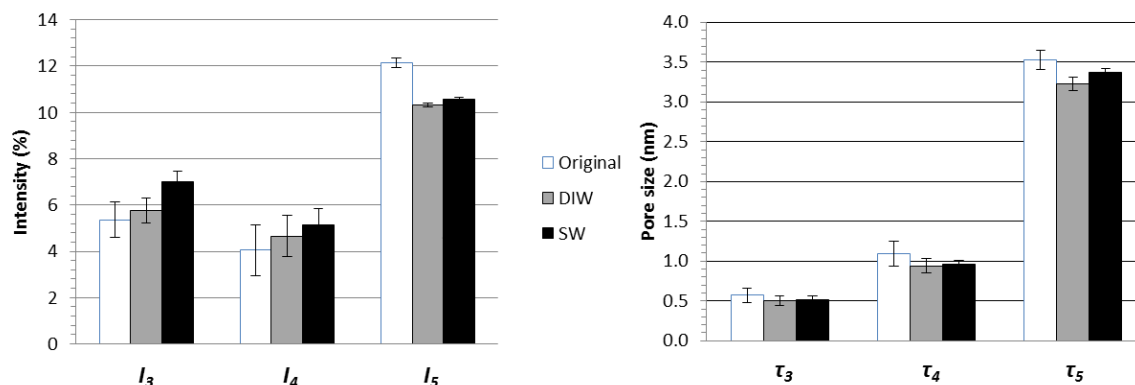

Figure 5: PALS results for the intensities (I_3, I_4 and I_5) and pore sizes calculated from corresponding lifetimes (τ_3, τ_4 and τ_5) of ZIF-8.

SEM

The materials were observed for physical changes upon DI water and seawater as shown in Figure 6 and 7 for SAPO-34 and ZIF-8 respectively. For SAPO-34, the sample before DI water and seawater exposure (Figure 6a) displayed the typical cubic/rectangular shape of chabazite (SAPO-34 topology). Crystals in the range of 1-3 µm were observed. The morphology was preserved after water and seawater treatment (Figures 6b and 6c). As shown in Figure 7, all three ZIF-8 samples show the typical hexagonal –like morphologies. Crystal size remained relatively constant for the three samples between 0.4nm and 0.6nm regardless of exposure to DI water or seawater.
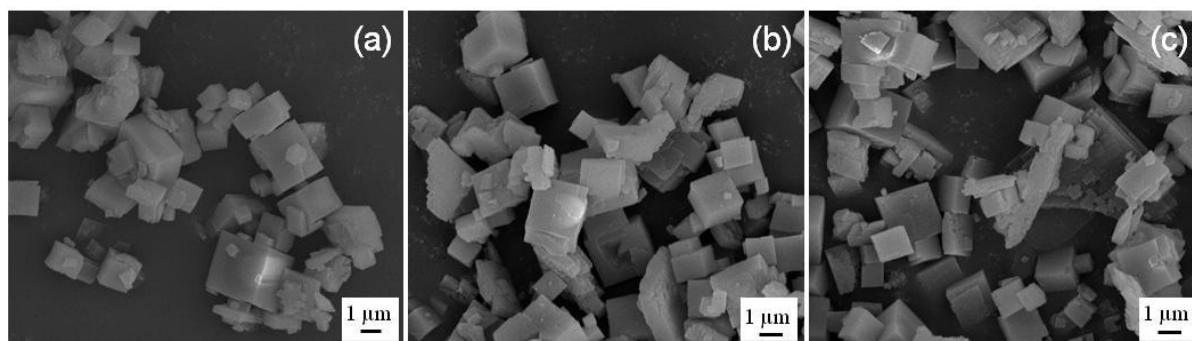

Figure 6: SEM images of SAPO-34 crystals: (a) before, (b) after exposure to DI water and (c) after exposure to seawater for 48 hours.
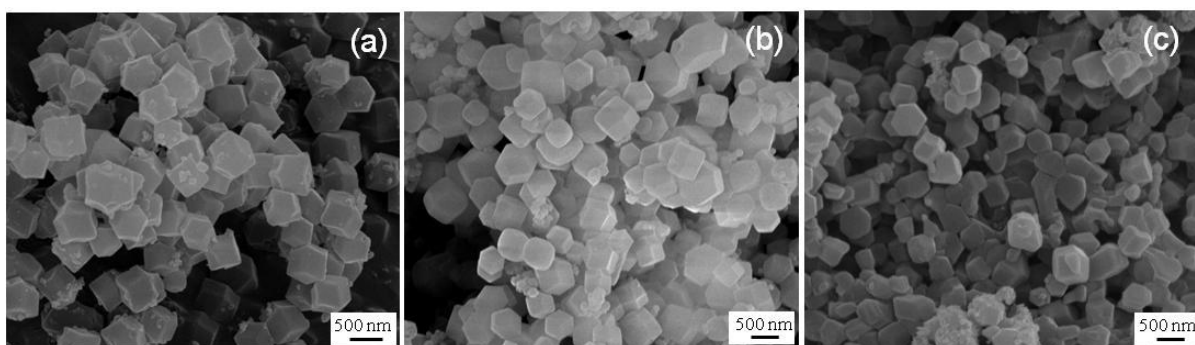
Figure 7: SEM images of ZIF-8 crystals: (a) before, (b) after exposure to DI water and (c) after exposure to seawater for 48 hours.

Membrane desalination

The final aspect of this study was to explore the potential for SAPO-34 and ZIF-8 to function as desalination membranes. The desalination test for the SAPO-34 and ZIF-8 membranes from this study are shown in Table 4. For the SAPO-34 membranes, applying pressures up to 700kPa did not lead to any significant permeation when fed with saline water (3,000 mg/L NaCl). The osmotic pressure of the NaCl feed solution is 227 kPa and is thus well in excess of the osmotic pressure to cause reverse osmosis. A test was also conducted on the first SAPO-34 membrane (#1) with pure water (DI water) which revealed no measurable flux. Our system is capable of measuring as low as 0.01 kg/m^2/h of liquid flow, so with this and no observed liquid evolution after 48 hours when fed with DI water, or 72 hours when fed with the NaCl solution, we conclude that the SAPO-34 was impermeable to liquid water. The second SAPO-34 membrane (#2) showed a very small liquid permeation, but this contained the same concentration of salt and therefore must have permeated in defects large enough to accommodate ions. SAPO-34 has a pore size of 0.38nm reported in literature [30], or 0.23nm by PALS in our work, meaning that the resistance of water through the structure with pores small enough to reject ions is too great to be conveniently driven by total pressure gradient. Compared to commercial reverse osmosis (RO) membranes which are considered dense, but are highly effective at permeating water under pressure, it is possible that our membrane's thickness (~8 μm) was too great compared to state of the art RO membranes (~0.2 μm). Further to this, although RO membranes are considered non-porous, the hydrophilic polyamide structure can accommodate water via swelling of the flexible aromatic polyamide structure, whereas SAPO-34 is a highly rigid purely inorganic structure and is thus not subject to structural alteration to accommodate water. Regardless, the SAPO-34 membrane structure was intact with essentially no contribution from permeation from grain boundaries. As in reverse osmosis, pressure driven separation is a key opportunity for membrane technology, however pervaporation of water (which hasn't been studied here) is clearly possible and driven by heat (temperature) [49].

The ZIF-8 membrane on the other hand did give a very high liquid permeation result. The first ZIF-8 membrane (#1) yielded a flux of 600 kg/m^2/h at 150kPa. After 30 minutes of permeation, we measured a NaCl rejection of 6.3%. The second ZIF-8 membrane (#2) showed a similar high flux result, but no salt concentration difference across the membrane. This is the first known reverse osmosis test in a ZIF-8 membrane, however the result is not promising for practical desalination applications requiring >90% rejection of NaCl. As presented in Figure 1, the aperture size of ZIF-8 that is widely reported of 0.34nm [15] leads to the intuitive view that ZIF-8 should block ions and

14

permeate water, which was also determined by simulation [29]. We measured a pore size by PALS of 0.55nm which may be indicative of the mean pore size that is more relevant to permeation. PALS detected larger pores in the membrane that would contribute to non-selective flow of salt water through the membrane. The slight loss of Zn that occurred in the presence of water may have contributed to the loss of selective pores and compromised the membrane's performance for desalination. This defect free property is essential for a working membrane, but not when used as sorbents [39, 40].

Table 4: Desalination test results for the SAPO-34 and ZIF-8 membranes. Feed NaCl solution concentration 3,000 mg/L. Tests performed at room temperature. Permeate pressure atmospheric.

Membrane	Feed pressure (kPa)	Flux (kg/m^2/h)	Salt rejection (%)
SAPO-34 #1	700	< 0.01	NA
SAPO-34 #2	500	0.34	0
ZIF-8 #1	150	600	6
ZIF-8 #2	200	118	0

We have therefore found that while SAPO-34 and ZIF-8 materials are structurally stable in DI water and seawater, their function as membrane films is impacted by their ability to conduct water (i.e. the case for SAPO-34) or prevent even slight mass losses of the material (i.e. the case for ZIF-8). While these structures appear unsuitable for reverse osmosis desalination, two other predominantly inorganic microporous materials, i.e. MFI-type zeolite and hybrid amorphous silica, have exhibited stable water permeation and salt rejection in reverse osmosis mode. MFI-type zeolite membranes have been shown to give salt rejections of 82% (7,000 kPa, 3,000 mg/L NaCl feed) [50] while hybrid silica membranes have been shown to give salt rejections exceeding 97% (1,150 kPa, 2,000 mg/L NaCl feed) [51]. So while this proves the desalination effect is achievable on inorganic based materials, SAPO-34 and ZIF-8 structures which possess the apparent physical property to diffuse water and reject salts in their native forms (Figure 1), appear to be unsuitable for reverse osmosis desalination. Future development on these materials for this application could involve design of well intergrown and robust membranes. Despite the need for such improvement, the performance needs to demonstrate a benefit over existing nanotechnologies as well as those which show promise but are still emerging. In a review of water treatment membrane nanotechnologies by Pendergast and Hoek in 2011, it was determined that zeolite membranes are far from commercial reality and offer small to moderate performance enhancements [52]. Indeed an estimate in 2013 of the cost of MFI-type zeolite membranes fabricated at a large scale come to US$2,700 per m^2, which is two orders or magnitude more expensive than their polymer counterparts [53]. However it was also stated that due to the material uniqueness of zeolites, their application as membranes for water treatment is an intriguing area of science and which could lead to interesting niche applications. So while at present zeolite membranes (including the SAPO-34 and ZIF-8 types in this study) in conventional desalination application appears far from commercial reality, bench testing and materials improvements are justified to explore novel material properties and unique effects.

4. Conclusions

This work has presented findings of the behaviour of common seawater cations for two novel desalination materials, SAPO-34 and ZIF-8. SAPO-34 released a minor quantity of ions into deionised water, but released a large quantity of Al which was replaced to a slight extent by other monovalent and divalent cations. XRD results demonstrated the robustness of the SAPO-34 structure in the presence of deionised water and seawater, with the majority of change to the porous structure occurring due to collapse of larger pores, mostly in the mesopore domain, due to capillary forces. The study on ZIF-8 materials showed a large release of Zn, even in deionised water. However this loss did not lead to structural instability detected by XRD or SEM images of the material which appeared to remain intact. Despite the finding that SAPO-34 and ZIF-8 maintained their crystal structures after exposure to fresh or sea water, neither membrane performed effectively for reverse osmosis desalination. Interestingly, it was found that, in powder form, SAPO-34 preferentially expelled the larger Al ions to accommodate smaller divalent, and to a larger extent monovalent ions, into the structure. On the other hand, the SAPO-34 membranes were unable to permeate a practically measureable amount of desalinated water, while ZIF-8 provided substantial permeation but at an unsatisfactory salt rejection. Therefore, we have found that while SAPO-34 and ZIF-8 materials are highly stable under aqueous environments including seawater, its performance as membrane material needs improvement if they were to be used for membrane desalination by reverse osmosis. This improvement can be potentially achieved by developing well intergrown and robust membranes.

5. Acknowledgement

6. References

[1]   R. Semiat, Energy Issues in Desalination Processes, Environmental Science & Technology, 42 (2008). 8193-8201.
[2]   W.B. Samuel de Lint, T. Zivkovic, N.E. Benes, H.J.M. Bouwmeester, and D.H.A. Blank, Electrolyte retention of supported bi-layered nanofiltration membranes, Journal of Membrane Science, 277 (2006). 18-27.
[3]   M.C. Duke, S. Mee, and J.C. Diniz da Costa, Performance of porous inorganic membranes in non-osmotic desalination, Water Research, 41 (2007). 3998-4004.
[4]   M.C. Duke, J. O'Brien-Abraham, N. Milne, B. Zhu, J.Y.S. Lin, and J.C. Diniz da Costa, Seawater desalination performance of MFI type membranes made by secondary growth, Separation and Purification Technology, 68 (2009). 343-350.
[5]   L. Li, J. Dong, T.M. Nenoff, and R. Lee, Reverse osmosis of ionic aqueous solutions on aMFI zeolite membrane, Desalination, 170 (2004). 309-316.
[6]   L. Li, J. Dong, T.M. Nenoff, and R. Lee, Desalination by reverse osmosis using MFI zeolite membranes, Journal of Membrane Science, 243 (2004). 401-404.

[7]   L. Li, N. Liu, B. McPherson, and R. Lee, Influence of counter ions on the reverse osmosis through MFI zeolite membranes: implications for produced water desalination, Desalination, 228 (2008). 217-225.

[8]   N. Liu, L. Li, B. McPherson, and R. Lee, Removal of organics from produced water by reverse osmosis using MFI-type zeolite membranes, Journal of Membrane Science, 325 (2008). 357-361.

[9]   L. Li, J. Dong, and T.M. Nenoff, Transport of water and alkali metal ions through MFI zeolite membranes during reverse osmosis, Separation and Purification Technology, 53 (2007). 42-48.

[10]   B. Zhu, Z. Hong, N. Milne, C.M. Doherty, L. Zou, Y.S. Lin, A.J. Hill, X. Gu, and M. Duke, Desalination of seawater ion complexes by MFI-type zeolite membranes: Temperature and long term stability, Journal of Membrane Science, 453 (2014). 126-135.

[11]   B. Zhu, D.T. Myat, J.-W. Shin, Y.-H. Na, I.-S. Moon, G. Connor, S. Maeda, G. Morris, S. Gray, and M. Duke, Application of robust MFI-type zeolite membrane for desalination of saline wastewater, Journal of Membrane Science, 475 (2014). 167-174.

[12]   M. Kazemimoghadam, New nanopore zeolite membranes for water treatment, Desalination, 251 (2010). 176-180.

[13]   E.R. Nightingale, Phenomenological Theory of Ion Solvation. Effective Radii of Hydrated Ions, The Journal of Physical Chemistry, 63 (1959). 1381-1387.

[14]   R. Szostak, Molecular Sieves, Principles of Synthesis and Identification. 1989, New York: van Nostrand Reinhold.

[15]   K.S. Park, Z. Ni, A.P. Cote, J.Y. Choi, R. Huang, F.K. Uribe-Romo, H.K. Chae, M. O'Keeffe, and O.M. Yaghi, Exceptional Chemical and Thermal Stability of Zeolitic Imidazolate Frameworks, Proceedings of the National Academy of Sciences of the USA, 103 (2006). 10186-10191.

[16]   H. Hayashi, A.P. Côté, H. Furukawa, M. O'Keeffe, and O.M. Yaghi, Zeolite A Imidazolate Frameworks, Nature Materials, 6 (2007). 501-506.

[17]   R. Banerjee, A. Phan, B. Wang, C. Knobler, H. Furukawa, M. O'Keeffe, and O.M. Yaghi, High-Throughput Synthesis of Zeolitic Imidazolate Frameworks and Application to CO2 Capture, Science, 319 (2008). 939-943.

[18]   B. Wang, A.P. Côté, H. Furukawa, M. O'Keeffe, and O.M. Yaghi, Colossal Cages in Zeolitic Imidazolate Frameworks as Selective Carbon Dioxide Reservoirs, Nature, 453 (2008). 207-211.

[19]   S.R. Venna and M.A. Carreon, Highly Permeable Zeolite Imidazolate Framework-8 Membranes for CO2/CH4 Separation, Journal of the American Chemical Society, 132 (2010). 76-78.

[20]   H. Bux, F. Liang, Y. Li, J. Cravillon, M. Wiebcke, and J.r. Caro, Zeolitic Imidazolate Framework Membrane with Molecular Sieving Properties by Microwave-Assisted Solvothermal Synthesis, Journal of the American Chemical Society, 131 (2009). 16000-16001.

[21]   Y. Liu, E. Hu, E.A. Khan, and Z. Lai, Synthesis and characterization of ZIF-69 membranes and separation for CO2/CO mixture, Journal of Membrane Science, 353 (2010). 36-40.

[22]   A. Huang, H. Bux, F. Steinbach, and J. Caro, Molecular-Sieve Membrane with Hydrogen Permselectivity: ZIF-22 in LTA Topology Prepared with 3-Aminopropyltriethoxysilane as Covalent Linker, Angewandte Chemie International Edition, 49 (2010). 4958-4961.

[23]   Y. Li, F. Liang, H. Bux, W. Yang, and J. Caro, Zeolitic imidazolate framework ZIF-7 based molecular sieve membrane for hydrogen separation, Journal of Membrane Science, 354 (2010). 48-54.

[24]   Y.-S. Li, H. Bux, A. Feldhoff, G.-L. Li, W.-S. Yang, and a.J. Caro, Controllable Synthesis of Metal–Organic Frameworks: From MOF Nanorods to Oriented MOF Membranes, Advanced Materials, 22 (2010). 3322–3326.

[25]   M.C. McCarthy, V. Varela-Guerrero, G.V. Barnett, and H.K. Jeong, Synthesis of zeolitic imidazolate framework films and membranes with controlled microstructures, Langmuir, 26 (2010). 14636-41.

[26] A. Huang and J. Caro, Covalent Post-Functionalization of Zeolitic Imidazolate Framework ZIF-90 Membrane for Enhanced Hydrogen Selectivity, Angewandte Chemie International Edition, 50 (2011). 4979-4982.

[27] H. Bux, A. Feldhoff, J. Cravillon, M. Wiebcke, Y.S. Li, and J. Caro, Oriented zeolitic imidazolate framework-8 membrane with sharp H2/C3H8 molecular sieve separation, Chemistry of Materials, 23 (2011). 2262.

[28] Y. Pan, Y. Liu, G. Zeng, L. Zhao, and Z. Lai, Rapid synthesis of zeolitic imidazolate framework-8 (ZIF-8) nanocrystals in an aqueous system, Chemical Communications, 47 (2011). 2071-2073.

[29] Z. Hu, Y. Chen, and J. Jiang, Zeolitic imidazolate framework-8 as a reverse osmosis membrane for water desalination: Insight from molecular simulation, The Journal of Chemical Physics, 134 (2011).

[30] S. Li, J.L. Falconer, and R.D. Noble, SAPO-34 membranes for CO2/CH4 separation, Journal of Membrane Science, 241 (2004). 121-135.

[31] L. Hertäg, H. Bux, J. Caro, C. Chmelik, T. Remsungnen, M. Knauth, and S. Fritzsche, Diffusion of CH4 and H2 in ZIF-8, Journal of Membrane Science, 377 (2011). 36-41.

[32] B. Zhu, L. Zou, C.M. Doherty, A.J. Hill, Y.S. Lin, X. Hue, H. Wang, and M. Duke, Investigation of the effects of ion and water interaction on structure and chemistry of silicalite MFI type zeolite for its potential use as a seawater desalination membrane, Journal of Materials Chemistry, 20 (2010). 4675-4683.

[33] S.J. Tao, Journal of Chemical Physics, 56 (1972). 5499-5510.

[34] M. Eldrup, D. Lightbody, and J.N. Sherwood, The temperature dependence of positron lifetimes in solid pivalic acid, Chemical Physics, 63 (1981). 51-58.

[35] T.L. Dull, W.E. Frieze, D.W. Gidley, J.N. Sun, and A.F. Yee, Determination of Pore Size in Mesoporous Thin Films from the Annihilation Lifetime of Positronium, The Journal of Physical Chemistry B, 105 (2001). 4657-4662.

[36] S.R. Venna and M. A.Carreon, Langmuir, 27 (2011). 2888-2894.

[37] B. Zhu, C.M. Doherty, X. Hu, A.J. Hill, L. Zou, Y.S. Lin, and M. Duke, Designing hierarchical porous features of ZSM-5 zeolites via Si/Al ratio and their dynamic behavior in seawater ion complexes, Microporous and Mesoporous Materials, 173 (2013). 78-85.

[38] J. Cravillon, S. Münzer, S.-J. Lohmeier, A. Feldhoff, K. Huber, and M. Wiebcke, Rapid Room-Temperature Synthesis and Characterization of Nanocrystals of a Prototypical Zeolitic Imidazolate Framework, Chemistry of Materials, 21 (2009). 1410-1412.

[39] D. Ge and H.K. Lee, Zeolite imidazolate frameworks 8 as sorbent and its application to sonication-assisted emulsification microextraction combined with vortex-assisted porous membrane-protected micro-solid-phase extraction for fast analysis of acidic drugs in environmental water samples, Journal of Chromatography A, 1257 (2012). 19-24.

[40] D. Ge and H.K. Lee, Water stability of zeolite imidazolate framework 8 and application to porous membrane-protected micro-solid-phase extraction of polycyclic aromatic hydrocarbons from environmental water samples, Journal of Chromatography A, 1218 (2011). 8490-8495.

[41] S.R. Venna and M.A. Carreon, Synthesis of SAPO-34 Crystals in the Presence of Crystal Growth Inhibitors, J. Phys. Chem. B, 112 (2008). 16261-16265.

[42] M.C. Duke, S.J. Pas, A.J. Hill, Y.S. Lin, and J.C. Diniz da Costa, Exposing the Molecular Sieving Architecture of Amorphous Silica Using Positron Annihilation Spectroscopy, Advanced Functional Materials, 18 (2008). 3818-3826.

[43] T. Niimi, H. Nagasawa, M. Kanezashi, T. Yoshioka, K. Ito, and T. Tsuru, Preparation of BTESE-derived organosilica membranes for catalytic membrane reactors of methylcyclohexane dehydrogenation, Journal of Membrane Science, 455 (2014). 375-383.

[44] X. Ma, H. Wang, H. Wang, J.O. Brien-Abraham, and Y.S. Lin, Pore structure characterization of supported polycrystalline zeolite membranes by positron annihilation spectroscopy, Journal of Membrane Science, 477 (2015). 41-48.

[45] A. Cabral-Prieto, I. García-Sosa, J. Jiménez-Becerril, M. Solache-Ríos, and S. Bulbulian, Ortho-positronium annihilation in the Na+, Co(II) and Mn(II) A-type zeolites, Microporous and Mesoporous Materials, 69 (2004). 109-118.

[46] Z.E. Hughes, L.A. Carrington, P. Raiteri, and J.D. Gale, A Computational Investigation into the Suitability of Purely Siliceous Zeolites as Reverse Osmosis Membranes, The Journal of Physical Chemistry C, 115 (2011). 4063–4075.

[47] G. Consolati, M. Mariani, R. Millini, and F. Quasso, Investigation on the porosity of zeolite NU-88 by means of positron annihilation lifetime spectroscopy, Nuclear Instruments and Methods in Physics Research Section B: Beam Interactions with Materials and Atoms, 267 (2009). 2550-2553.

[48] K.S. Park, Z. Ni, A.P. Cote, J.Y. Choi, R. Huang, F.J. Uribe-Romo, H.K. Chae, M. O'Keeffe, and O.M. Yaghi, Exceptional chemical and thermal stability of zeolitic imidazolate frameworks, Proceedings of the National Academy of Sciences, 103 (2006). 10186-10191.

[49] T.C. Bowen, R.D. Noble, and J.L. Falconer, Fundamentals and applications of pervaporation through zeolite membranes, Journal of Membrane Science, 245 (2004). 1-33.

[50] B. Zhu, J. Kim, Y.-H. Na, I.-S. Moon, G. Connor, S. Maeda, G. Morris, S. Gray, and M. Duke, Temperature and Pressure Effects of Desalination Using a MFI-Type Zeolite Membrane, Membranes, 3 (2013). 155-168.

[51] R. Xu, J. Wang, M. Kanezashi, T. Yoshioka, and T. Tsuru, Development of Robust Organosilica Membranes for Reverse Osmosis, Langmuir, 27 (2011). 13996-13999.

[52] M.M. Pendergast and E.M.V. Hoek, A review of water treatment membrane nanotechnologies, Energy & Environmental Science, 4 (2011). 1946-1971.

[53] Y.S. Lin and M.C. Duke, Recent progress in polycrystalline zeolite membrane research, Current Opinion in Chemical Engineering, 2 (2013). 209-216.